IEEE Access
Multidisciplinary | Rapid Review | Open Access Journal

Received December 30, 2019, accepted January 20, 2020, date of publication January 30, 2020, date of current version February 7, 2020.

Digital Object Identifier 10.1109/ACCESS.2020.2970473

A Low-Profile Dual-Band Dual-Polarized Antenna With an AMC Reflector for 5G Communications

QINGCHONG LIU[1,*], HUI LIU[1,2,*], (Member, IEEE), WANG HE[1], AND SAILING HE[1,2,3], (Fellow, IEEE)

[1]Center for Optical and Electromagnetic Research, National Engineering Research Center for Optical Instruments, Zhejiang University, Hangzhou 310058, China
[2]Ningbo Research Institute, Zhejiang University, Ningbo 315100, China
[3]Department of Electromagnetic Engineering, School of Electrical Engineering, KTH Royal Institute of Technology, S-100 44 Stockholm, Sweden

Corresponding author: Sailing He (sailing@kth.se)

*Qingchong Liu and Hui Liu contributed equally to this work.

This work was supported in part by the National Key Research and Development Program of China under Grant 2018YFC1407500, and in part by the National Natural Science Foundation of China under Grant 11621101.

ABSTRACT A low-profile dual-band dual-polarized antenna with an artificial magnetic conductor (AMC) reflector is proposed for 5G communications. The antenna consists of a pair of crossed dual-polarized dual-band bowtie dipoles and a dual-band AMC reflector. By introducing trapezoidal slots and U-shaped slots on the bowtie dipoles, miniaturization and dual-band characteristics are achieved. Moreover, T-shaped feeding structures are utilized to broaden the bandwidth of the bowtie dipoles. By adopting a dual-band AMC reflector instead of a conventional perfect electric conductor (PEC) reflector, the distance between the radiator and the reflector can be reduced from $0.25\lambda_0$ to $0.08\lambda_0$ (where λ_0 is the free-space wavelength at 3.5 GHz). The radiator can maintain the impedance bandwidth and a high gain can also be achieved, even if it is close to the AMC reflector. A geometrical optics model is used to explain the mechanism of the AMC. The optimal parameters of the AMC depend on the antenna operating frequency and the distance between the radiator and the reflector. Measurements show that the proposed dual-band antenna has an impedance bandwidth of 19.8% (3.14-3.83 GHz) and 13.2% (4.40-5.02 GHz), covering the sub-6 GHz frequency spectra of 5G mobile communications. The peak gain is 7.1 dBi in the lower band and 8.2 dBi in the upper band. Port isolation better than 20 dB is achieved. The proposed antenna can be used alone for 5G indoor base station, or as the element of an array for 5G outdoor base station.

INDEX TERMS 5G, artificial magnetic conductor (AMC), dual-band antenna, dual polarization, low profile.

I. INTRODUCTION

Recently, there has been an increasing interest in the fifth generation (5G) mobile communication, which offers faster speeds and lower latency than ever before on smartphones and other devices [1]. Since 2016, the band from 3.4–3.8 GHz has been allocated for 5G trials in the European Union (EU). In China, 3.3-3.6 GHz and 4.8-5.0 GHz bands have been allocated as the sub-6 GHz frequency spectra for 5G mobile communication [2]. As one of the most important components in a 5G communication system, antennas for 5G base stations have attracted much attention [3]–[11]. Dual-polarized antennas are widely used in wireless communication systems to increase the spectrum efficiency and channel capacity. Moreover, dual-polarized antennas can not only reduce the multipath fading and installation space, but also overcome the issue of polarization mismatch between the transmitter and the receiver. Base station antennas should have the following characteristics: broadband/multiband bandwidth, dual polarizations, high isolation, low profile, high gain, stable radiation pattern and high front-to-back ratio, etc. However, there is usually a trade-off between the radiation performance and the dimensions of the antenna.

In order to realize unidirectional radiation with high gain, a base station antenna is usually backed with a perfect electric conductor (PEC) reflector [12]–[16]. However, if the antenna was positioned close to the PEC reflector, the mirror currents flowing in the opposite direction would cancel the radiation of the currents on the antenna, and consequently the radiation performance would severely deteriorate. Thus, a sufficient gap between the antenna and the PEC reflector is usually required, which is about 1/4 λ_0 (where λ_0 is the free-space wavelength at the central working frequency). To enhance the performance of the antenna while maintaining

The associate editor coordinating the review of this manuscript and approving it for publication was Raghvendra Kumar Chaudhary.

a low profile, an artificial magnetic conductor (AMC) reflector or a metasurface reflector has been introduced in the antenna design [17]–[27]. A low-profile dual-band dual-polarized antenna with AMC surface for wireless local area network (WLAN) applications was presented in [18], and an AMC operating with 90° reflection-phase bandwidth of 1.64–2.88 GHz was designed in [21]. However, the antennas with complex feeding structure in [18] and [21] are of three-layer structures, and are challenging to manufacture. In [22], a low-profile dual-polarized antenna MIMO array was presented, and the MIMO array was backed by a single-layer AMC structure with circle metallic unit cells, allowing the antenna to yield a low profile of $0.067\lambda_0$. However, the antenna has only one single working band from 2.4 to 3 GHz. In [24] and [25], a metasurface reflector was utilized to enhance the bandwidth and gain of the single-band wideband circularly-polarized antenna while maintaining a low profile. In [26], a low-profile dual-band dual-mode and dual-polarized antenna based on AMC was presented. Monopole-like omnidirectional linear polarization (LP) radiation and patch-like unidirectional circularly polarized (CP) radiation were achieved for two bands by loading an AMC structure with a 90° reflection phase difference between 1.38 and 1.57 GHz. In [27], three compact planar antennas enabled by interdigitated capacitor-loaded metasurfaces were introduced. The first two LP antenna designs enhance the gain and bandwidth by virtue of a metasurface with singly and doubly loaded interdigitated capacitors, respectively. Furthermore, a compact CP antenna was designed by placing an anisotropic metasurface beneath an LP monopole feed antenna.

In this paper we propose a low-profile dual-band dual-polarized antenna with a dual-band AMC reflector for sub-6 GHz 5G applications. The proposed antenna, with a size of $0.93\lambda_0 \times 0.93\lambda_0 \times 0.13\lambda_0$ (where λ_0 is the free-space wavelength at 3.5 GHz), has a measured impedance bandwidth of 19.8% (3.14-3.83 GHz) and 13.2% (4.40-5.02 GHz), covering both 3.3-3.8 GHz and 4.8-5.0 GHz bands, which are sub-6 GHz frequency spectra of 5G mobile communication. A port isolation better than 20 dB is achieved. Meanwhile, the peak gain of 7.1 dBi in the lower band and 8.2 dBi in the upper band are also achieved. The proposed antenna (a single antenna on a periodic AMC substrate) can be used alone for 5G indoor base station, or used as the element of an array for 5G outdoor base station.

II. ANTENNA CONFIGURATION AND WORKING MECHANISM

A. CONFIGURATION OF THE PROPOSED ANTENNA

Fig. 1(a) and (b) show the configuration of the proposed dual-band dual-polarized antenna. The antenna consists of a pair of crossed dual-band bowtie dipoles (as the radiator), an AMC reflector, two feeding coaxial cables and four supporting posts. The crossed dipoles are suspended at a height H from the top of the AMC. Four nylon posts are used to support the radiator.

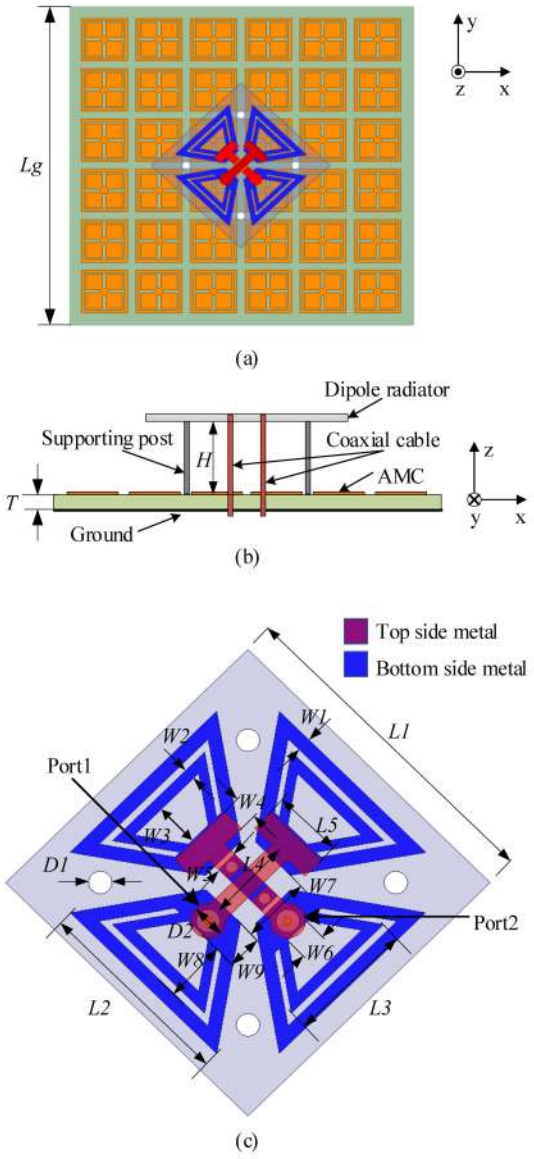

FIGURE 1. Configuration of the proposed antenna: (a) top view and (b) side view. (c) Top view of the dipole radiator.

The geometry of the dipole radiator is shown in Fig. 1(c). The radiator is printed on a 1.0 mm thick square FR-4 substrate with a relative permittivity of 4.4 and a loss tangent of 0.02. It is composed of two perpendicularly crossed bowtie dipoles for ±45° polarizations (as a dual-polarized radiator) and two crossed T-shaped coupling feed lines. Port1 is connected to +45° dipole to excite the +45° polarization and Port2 is connected to −45° dipole to excite the −45° polarization. The AMC reflector is geometrically symmetric, and thus is insensitive to the polarization and could maintain the polarization of the radiator. The dipoles are printed on the bottom side of the substrate, and two T-shaped coupling feed lines are printed on the top side of the same substrate. To avoid physical overlap/touching of the two crossed feed lines, the central section of the T-shaped feed line for

−45° polarization dipole is printed on the bottom side of the substrate. The sections on the top side are then connected to the central section on the bottom side through two metallic vias with a diameter of 1.0 mm. As shown in Fig. 1(b) and (c), the coaxial cables pass through the AMC. The outer conductor of the coaxial cables is soldered to one arm of the dipole at the bottom layer, and the inner conductor of the coaxial cables is directly connected to the T-shaped feed line at the top layer. The final dimensions of the proposed antenna are listed in Table 1. The simulated results in this paper are calculated with the commercial electromagnetic full-wave simulation software ANSYS HFSS [28].

TABLE 1. Dimensions of the proposed antenna.

Parameters	Value (mm)	Parameters	Value (mm)	Parameters	Value (mm)
D1	2.0	*L1*	29.2	*W1*	1.2
D2	3.0	*L2*	17.6	*W2*	1.0
H	7.0	*L3*	11.1	*W3*	3.8
La1	12.6	*L4*	7.4	*W4*	2.0
La2	10.6	*L5*	6.0	*W5*	1.9
La3	3.8	*Lg*	79.6	*W6*	2.4
La4	3.4	*Wa1*	0.4	*W7*	6.0
T	3.0	*Wa2*	0.8	*W8*	5.4
				W9	3.0

B. RADIATOR DESIGN

The evolutionary progression of the dual-band dipole radiator element is shown in Fig. 2. All these antennas in Fig. 2 have the same dimensions and the same substrate as the antenna in Fig. 1(c). The reflection coefficients of the antennas in Fig. 2 are shown in Fig. 3. A conventional bowtie antenna (denoted as "A" in Fig. 2) is initially adopted, which only resonates around 3.2 GHz. Then by loading a U-shaped slot on each arm of antenna A, an extra resonance occurs at 4.6 GHz, as shown in Fig. 3, and the dual-band operation is achieved on

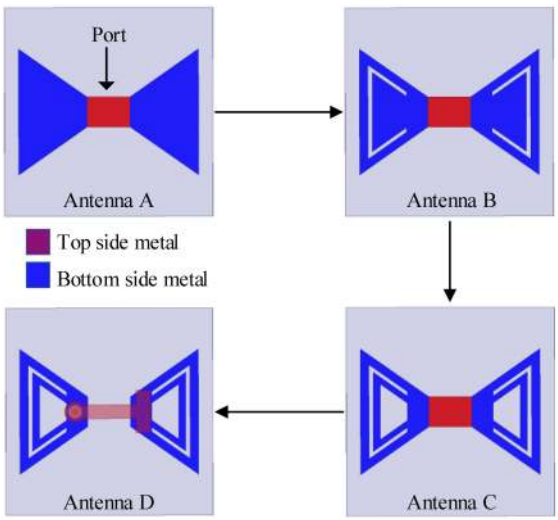

FIGURE 2. Evolutionary process of the radiating dipole element.

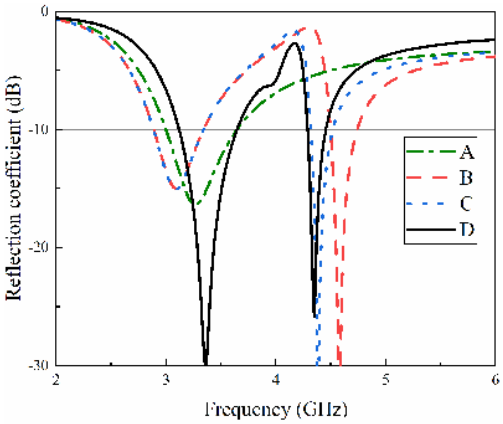

FIGURE 3. Reflection coefficients of the dipole elements.

antenna B. In order to reduce the upper resonant frequency, a trapezoidal slot is loaded on each arm of antenna B (see antenna C in Figure 2). Finally, an actual T-shaped feeding structure is added to antenna C, and thus antenna D gives a better reflection coefficient. As shown later that the second resonance will shift to a higher frequency when the radiator is brought close to an AMC. Thus, here we intentionally designed the second resonant frequency to be lower than the desired band 4.8-5.0 GHz.

C. AMC DESIGN

The geometry of the AMC unit cell is a square patch with four rectangular slots and a square ring, as shown in Fig. 4(a). The design of the AMC unit cell is inspired by [29]. The AMC is printed on an F4BTME-1/2 substrate [30] with a thickness of 3 mm, a relative permittivity of 4.4 and a loss tangent of 0.003. The bottom surface of the substrate is the metal ground. The simulated reflection phases of the dual-band AMC and the single-band AMC (without ring and slots) are shown in Fig. 4(b). The resonant frequency of the AMC corresponds to the reflection phase of 0°. The single-band AMC (without ring and slots) has only one resonant frequency around 6.0 GHz. After loading four square slots, the single-band AMC without ring gives a lower resonant frequency of 5.2 GHz, which is better for miniaturization. In order to achieve dual resonances, a square ring is added, and consequently an additional lower band centered at a resonant frequency of 3.6 GHz can be achieved by the final dual-band AMC. Comparing the dual-band AMC with the single-band AMC in Fig. 6, one can see that larger bandwidth of the AMC leads to larger bandwidth of the dual-band antenna.

A geometrical optics model has been used to explain the mechanism of the AMC reflector in [31]. The optimal parameters of the AMC depend on the antenna operating frequency and the distance between the radiator and the reflector. The desired reflection phase of the AMC can be determined by

$$\frac{2\pi f}{c}2H - \Phi = 2n\pi, \quad (n = 0, 1, 2, \cdots) \tag{1}$$

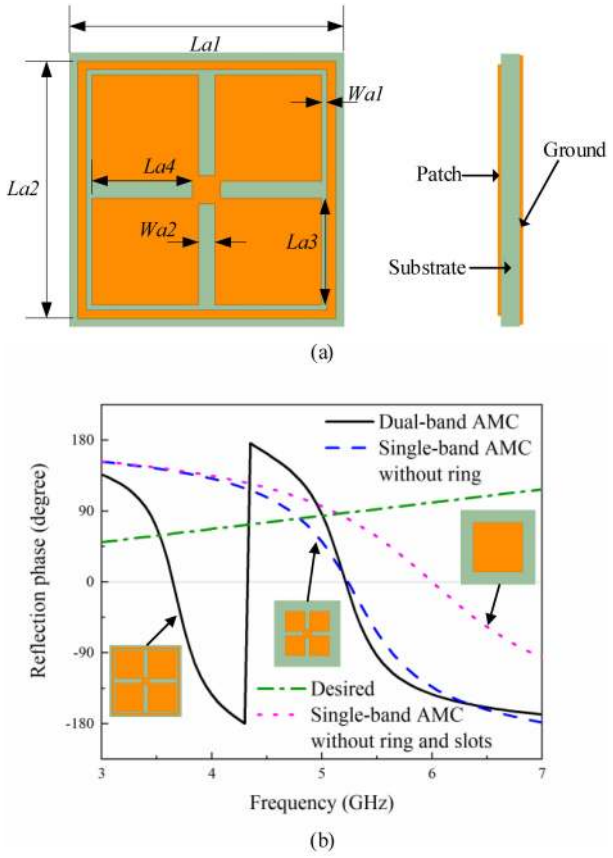

FIGURE 4. (a) Geometry of the AMC element and (b) simulated reflection phases for AMCs with/without ring/ slots.

where Φ, f, H and c represent the desired reflection phase of the AMC, the operating frequency, the distance between the radiator and the reflector, and the speed of light in vacuum, respectively. The desired reflection phase of the AMC calculated by (1) in case of $H = 7$ mm is plotted in Fig. 4(b). In this paper, the bandwidth of the AMC is defined as the range where the absolute value of the difference between the reflection phase of the AMC and the desired reflection phase calculated by (1) is less than 90°. Thus, the AMC bandwidth is 2.9-3.7 GHz and 4.5-5.2 GHz, covering the sub-6 GHz operating band of 5G in China.

Fig. 5(a) shows the simulated reflection phases of the dual-band AMC with different values of *La*2. The increase of *La*2 results in decrease of the lower-band resonant frequency, while the upper-band resonant frequency remains unchanged. As shown in Fig. 5(b)-(d), the upper-band resonant frequency decreases as the increase of *La*3, *La*4, or *Wa*2, while the lower-band resonant frequency remains unchanged. Therefore, the resonant frequency of the AMC can be easily tuned by varying the values of *La*2, *La*3, *La*4 and *Wa*2. According to (1), the reflection phases of the AMC at 3.5 GHz and 4.9 GHz can be calculated, and thus we can optimize the design parameters (e.g. *La*2) of the AMC. The optimal parameters of the AMC are also listed in Table 1.

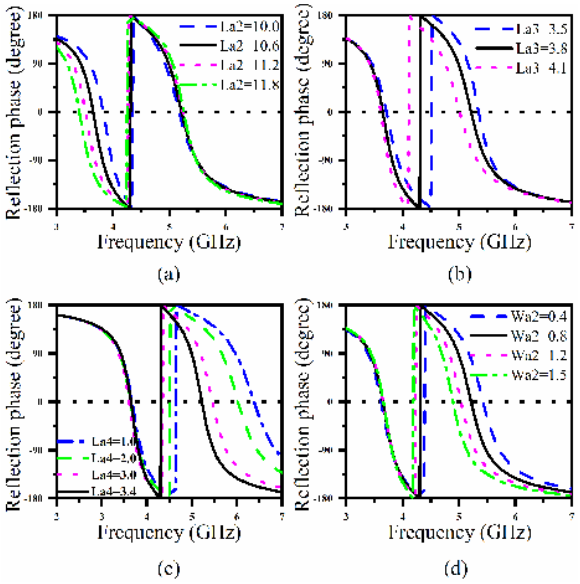

FIGURE 5. Reflection phases of the dual-band AMC for different (a) La2, (b) La3, (c) La4, and (d) Wa2.

D. ANALYSIS OF THE ANTENNA LOADED WITH AMC REFLECTOR

Fig. 6 shows the simulated S_{11} of the proposed dipole radiator with the PEC or the dual-band/single-band AMC reflector. The single-band AMC (without rings and slots) is designed to reach the desired reflection phase at 3.5 GHz. The dipole radiator without the reflector and with a perfect electric conductor (PEC) are also simulated for comparison. The detailed dimensions and performance of these antennas are shown in Table 2. The PEC reflector has the same size and the same distance ($H = 7$ mm) to the dipole radiator as the AMC reflector. Due to the symmetry of the antenna, the characteristics of port1 and port2 are similar, so only S_{11} is provided in Fig. 6. Here we see the upper-band resonant frequency of the antenna with the dual-band AMC reflector has been shifted to a higher frequency, and the upper-band

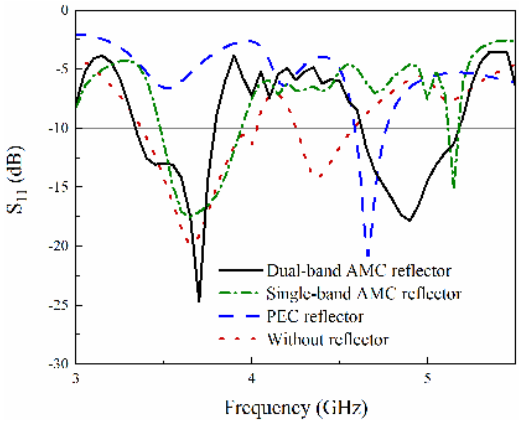

FIGURE 6. Simulated S 11 of the antenna with AMC/PEC reflector and without any reflector.

TABLE 2. Comparison of the propoed antenna with single/dual-band AMC reflector or without any reflector.

Antenna	Size (λ_0^3)	Bandwidth (GHz)	Gain (dBi)
Without reflector	0.34×0.34×0.01	3.37-4.02 4.25-4.57	2.3 & 1.5
PEC reflector	0.93×0.93×0.09	4.59-4.76	6.8 & 8.4
Single-band AMC reflector	0.93×0.93×0.13	3.47-3.93 5.12-5.18	8.1 & 7.6
Dual-band AMC reflector	0.93×0.93×0.13	3.33-3.79 4.62-5.18	8.2 & 7.8

bandwidth increases slightly, as compared with the antenna without the reflector. For comparison, when the single-band AMC reflector is used, but the impedance of the radiator can be maintained at the lower band, but the bandwidth of the radiator at the upper band is reduced (the upper-band resonant frequency is shifted slightly to a higher frequency). The impedance bandwidth of the dipole radiator with a PEC reflector degrades significantly, especially at the lower band, since $H = 7$ mm is much less than a quarter-wavelength at the lower band. The gain of the antenna with the AMC or PEC reflector is improved significantly, as shown in Fig. 7. In short, the AMC reflector enhanced the gain of the dipole radiator when it is close to the radiator.

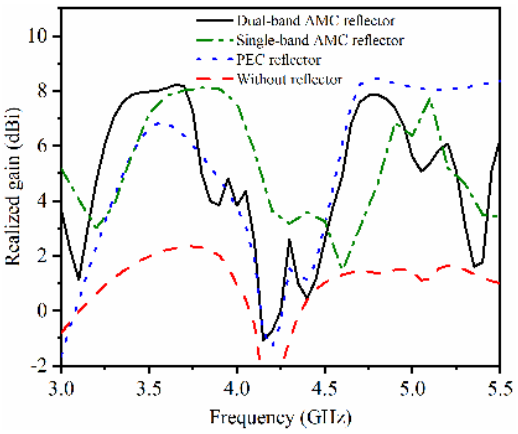

FIGURE 7. Simulated gains of the antenna with AMC/PEC reflector and without any reflector.

The distance (H) between the dipole radiator and the AMC reflector has a significant impact on the S-parameters, as shown in Fig. 8. When the value of H is too small (i.e. $H = 3$mm), the bandwidth is too narrow to cover the 5G frequency band. If the value of H is too large (i.e. $H = 11$mm), the antenna profile will increase. Here $H = 7$ mm is selected, as a trade-off between the performance and the dimension.

III. RESULTS AND DISCUSSION

The prototype of the proposed dual-band dual-polarized antenna with the AMC reflector is fabricated, as shown in Fig. 9. The simulated and measured S-parameters of the proposed antenna are shown in Fig. 10. Due to the small

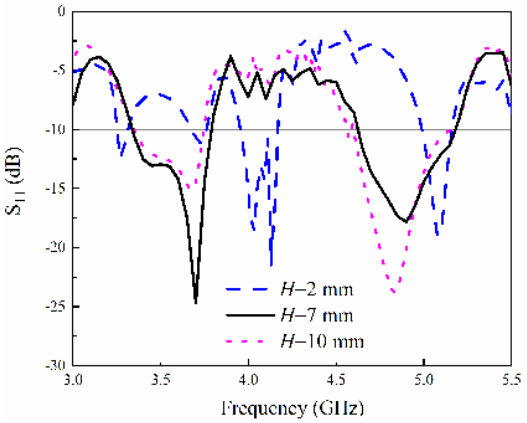

FIGURE 8. Simulated S11 of the proposed antenna with different H.

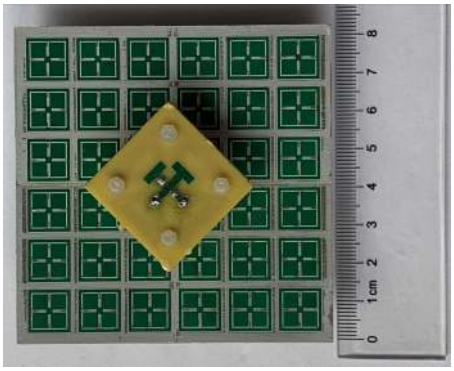

FIGURE 9. Fabricated prototype of the proposed antenna.

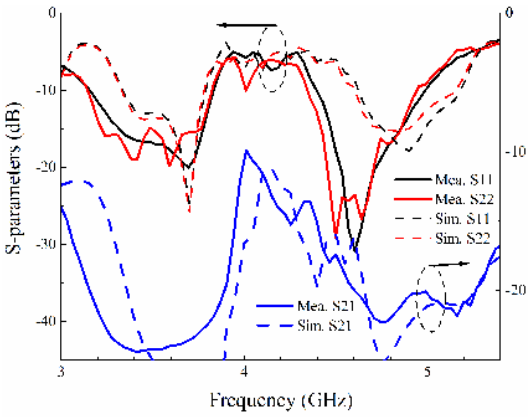

FIGURE 10. Simulated and measured S-parameters of the proposed antenna.

difference between the two T-shaped feeding lines, the reflection coefficient for port 1 and port 2 are slightly different. The measured impedance bandwidths for $|S_{11}| < -10$ dB are 3.14-3.83 GHz and 4.40-5.02 GHz, covering the 5G frequency bands in China (3.3-3.6 GHz and 4.8-5.0 GHz). Since the radiator and AMC have their own resonant frequencies and the nearby AMC will influence the radiator frequency, it is hard to make a design with a perfect impedance

match. Thus, the radiator needs to be optimized, after the radiator and the AMC reflector are separately designed at the operating bands. In fact, the length of the coaxial cables used in the fabricated prototype is much larger than that in the simulation, and the losses in the cables may result in less reflected energy. Thus, the simulated reflection coefficient is even larger than the measured one at the upper band. The measured and simulated port isolations are in good agreement with each other. The isolation between two ports is better than 20 dB in the 5G operating band. The measured and simulated second resonant frequencies have some shift in Fig. 10 because the actual relative permittivity of the substrate may be larger than the value (i.e. $\epsilon_r = 4.4$) provided by the vendor. To verify our conjecture, the simulated S_{11} for the proposed antenna with a substrate $\epsilon_r = 5.0$ is also calculated and shown in Fig. 11, from which we see that the simulated S_{11} curve agrees much better with the measured S_{11} when the relative permittivity of the substrate is assumed to be 5.0.

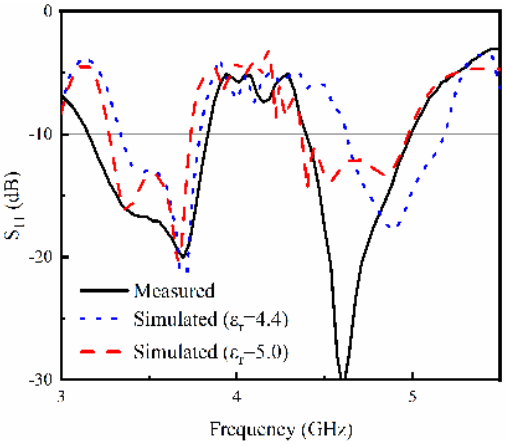

FIGURE 11. Measured and simulated S_{11} of the proposed antenna ($H = 7$ mm) with different permittivity of the radiator substrate.

Fig. 12 shows the measured and simulated normalized radiation patterns of the proposed antenna at 3.5 GHz and 4.9 GHz. Due to the symmetry of the antenna, only radiation

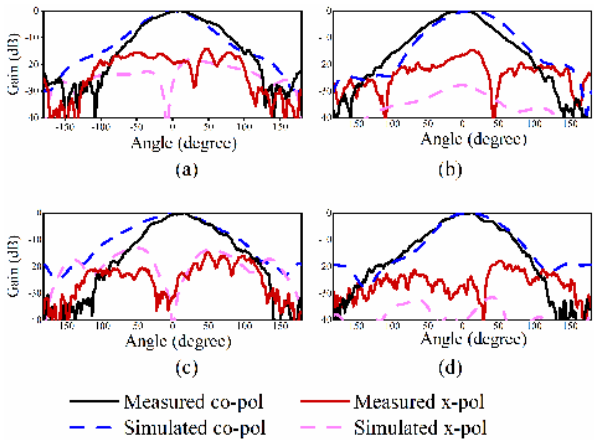

FIGURE 12. Simulated and measured normalized radiation patterns of the proposed antenna. (a) E-plane at 3.5GHz. (b) H-plane at 3.5GHz. (c) E-plane at 4.9GHz. (d) H-plane at 4.9GHz.

patterns with port 1 excited are presented. During the test, port1 of the proposed antenna is connected to the test cable and port2 is connected to a matched load. It is observed that the measured and simulated co-polarization radiation patterns agree well with each other at 3.5 GHz and 4.9 GHz. The discrepancy in the cross-polarization patterns is mainly caused by the limited accuracy in low level measurement and the errors in fabrication and assembly. The simulated radiation efficiency, the measured and simulated realized gains are shown in Fig. 13, where one sees that the radiation efficiency is better than 90% over the 5G operating bands. The measured realized gain can reach nearly 7.1 dBi and 8.2 dBi at the lower and upper operating bands, respectively. Since the actual permittivity of the substrate used in the fabrication is larger than the value (i.e. $\epsilon_r = 4.4$) provided by the vendor and used in the simulation, there is a frequency shift in the upper band between the measured and simulated gains (in case of $\epsilon_r = 4.4$). To further verify that the actual permittivity deviates from the design value (i.e. $\epsilon_r = 4.4$), the simulated gain of the proposed antenna with a substrate $\epsilon_r = 5.0$ is also calculated and plotted as the red dotted curve in Fig. 13. It can be seen from Fig. 13 that the simulated gain is more consistent with the measured gain when the relative permittivity of the substrate is assumed to be $\epsilon_r = 5.0$. The resonant frequency shift results in the sharp decrease of the measured gain in the upper band of 5G. However, the simulated gain (in case of $\epsilon_r = 4.4$) is nearly flat in the upper band (4.8 GHz - 5 GHz), and it can still show the validity of the antenna design.

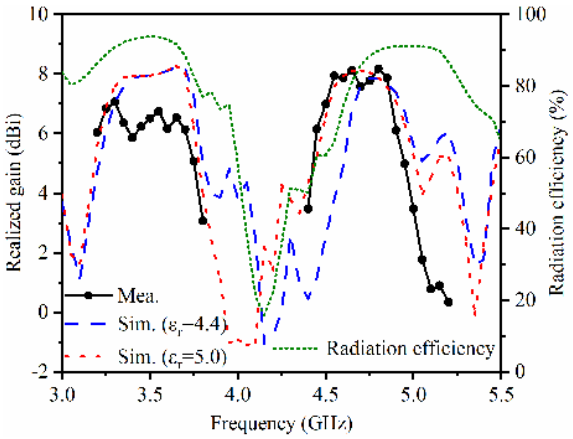

FIGURE 13. Simulated radiation efficiency, simulated and measured realized gain of the proposed antenna.

To verify that the proposed antenna is suitable for use as the antenna element in an array, a 1×4 array consisting of four elements of the proposed antenna is simulated, as shown in Fig. 14. The geometry of the array is depicted in Fig. 14(a). The element of the array has the same size as the proposed antenna. Fig. 14(b) shows the simulated S-parameters of the array. Due to the symmetry of the array, only the S-parameters related to the first two elements of the array are given. The simulated impedance bandwidths of $|S_{11}| < -10$ dB are 3.3-3.8 GHz and 4.6-5.1 GHz, covering the sub-6 GHz

TABLE 3. Comparison of the proposed antenna with some existing works.

References	Size (λ_0^3)	Bandwidth (GHz)	Isolation (dB)	Gain (dBi)	Polarization	Radiation efficiency
[5]	0.91×0.91×0.26	7.7% (2.5-2.7) +8.7% (3.3-3.6)	≥25	8.4	Dual	N/A
[12]	1.47×0.99×0.27	45% (1.7–2.7)	≥30	8.5	Dual	N/A
[13]	1.15×1.15×0.25	52% (1.7-2.9)	≥35	8.6	Dual	80%
[18]	0.87×0.87×0.09	15.6% (2.36–2.76) +9.3% (5.12– 5.62)	≥22	7.3	Dual	65%
[21]	1.39×1.10×0.14	56% (1.67–2.98)	≥25	7.3	Dual	86%
[22]	1.01×1.01×0.07	22% (2.4-3.0)	≥28	7	Dual	92%
[24]	0.72×0.72×0.16	26.5% (2.23–2.91)	≥14.5	7.02	CP	N/A
[25]	0.37×0.37×0.18	33.1% (2.18-3.04)	N/A	5.76	CP	N/A
This work	0.93×0.93×0.13	19.8% (3.14-3.83) +13.2% (4.40-5.02)	≥20	8.2	Dual	90%

λ_0 is the wavelength at the center frequency of the lower working band.

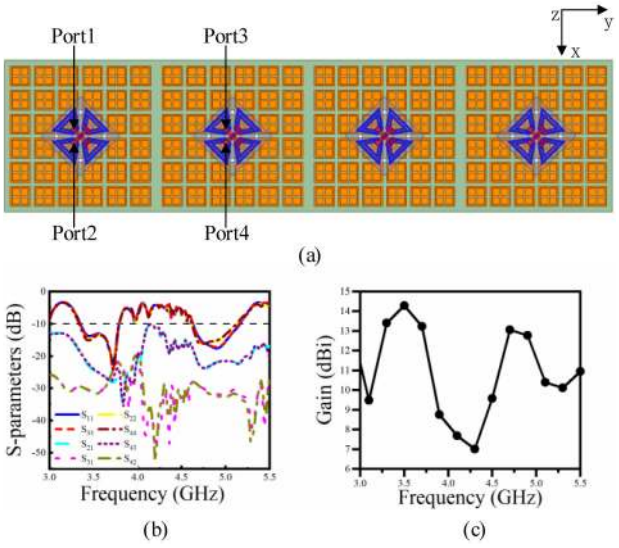

FIGURE 14. (a) Top view of the 1 × 4 array. (b) Simulated S-parameters of the array. (c) Simulated gain of the array.

frequency spectra of 5G mobile communications in China. The isolations are better than 20 dB over the operating bands. The gain of the array is simulated when all ports for +45° polarization are excited with equal amplitude and phase, and all ports for -45° polarization are connected to the matched load. Fig. 14(c) shows that the gains of the array are 14.3 dBi at 3.5 GHz and 12.8 dBi at 4.9 GHz. From the above simulating results, one sees that the proposed antenna is suitable for use in 5G base station array.

The proposed low-profile dual-band dual-polarized antenna with high gain can meet the requirement of 5G communication for sub-6 GHz bands in China. The performances of the proposed antenna are compared with some previously published antennas of similar kind in Table 3. The height of the proposed antenna is only $0.13\lambda_0$, which is lower than that in [5], [12], [13], [21], [24] and [25]. The total bandwidth of the proposed antenna is also larger than those in [5], [18], [22], and [24]. Moreover, the gain of the proposed antenna is etter than those in [18], [21]–[25]. The dual-band characteristic of the proposed antenna is beneficial to cover the 5G operating bands and to avoid the out-band interferences.

IV. CONCLUSION

A low-profile dual-band dual-polarized antenna has been designed, optimized, fabricated and measured. A dual-band AMC reflector has been used to replace the conventional PEC reflector to enhance the gain of the dual-band 5G base station antenna while maintaining a low profile. The proposed antenna, with a size of $0.93\lambda_0 \times 0.93\lambda_0 \times 0.13\lambda_0$ (where λ_0 is the free-space wavelength at central frequency 3.5 GHz of the lower working band), has the advantages of low profile and good impedance matching. It has an impedance bandwidth of 19.8% (3.14-3.83 GHz) and 13.2% (4.40-5.02 GHz) for $|S_{11}| < -10$ dB, covering the sub-6 GHz spectra of 5G mobile communications in China. The port isolation of the antenna is better than 20 dB within the 5G operating band. The measured realized gain can reach nearly 7.1 dBi and 8.2 dBi at the lower and upper operating bands, respectively. Therefore, the proposed antenna can be used alone for 5G indoor base station, or as the element of an array for 5G outdoor base station.

ACKNOWLEDGMENT

The authors would like to thank Dr. J. Evan for valuable discussion and Dr. Dong's team from Fragrant Mountain Microwave Co. Ltd (F&MM), China, for their helps in antenna performance measurement with automatic testing system.

REFERENCES

[1] M. Shafi, A. F. Molisch, P. J. Smith, T. Haustein, P. Zhu, P. De Silva, F. Tufvesson, A. Benjebbour, and G. Wunder, "5G: A tutorial overview of standards, trials, challenges, deployment, and practice," *IEEE J. Sel. Areas Commun.*, vol. 35, no. 6, pp. 1201–1221, Jun. 2017.

[2] *Notice of the Ministry of Industry and Information Technology on the Use of the 3300-3600 MHz and 4800-5000 MHz Bands in the Fifth Generation Mobile Communication System*. Accessed: Oct. 20, 2019. [Online]. Available: http://www.miit.gov.cn/n1146295/n1652858/n1652930/n3757020/c5907905/content.html

[3] A. Alieldin, Y. Huang, S. J. Boyes, M. Stanley, S. D. Joseph, Q. Hua, and D. Lei, "A triple-band dual-polarized indoor base station antenna for 2G, 3G, 4G and sub-6 GHz 5G applications," *IEEE Access*, vol. 6, pp. 49209–49216, 2018.
[4] P. I. Bantavis, C. I. Kolitsidas, T. Empliouk, M. Le Roy, B. L. G. Jonsson, and G. A. Kyriacou, "A cost-effective wideband switched beam antenna system for a small cell base station," *IEEE Trans. Antennas Propag.*, vol. 66, no. 12, pp. 6851–6861, Dec. 2018.
[5] Y. Liu, S. Wang, N. Li, J.-B. Wang, and J. Zhao, "A compact dual-band dual-polarized antenna with filtering structures for sub-6 GHz base station applications," *IEEE Antennas Wireless Propag. Lett.*, vol. 17, no. 10, pp. 1764–1768, Oct. 2018.
[6] K. R. Mahmoud and A. M. Montaser, "Performance of tri-band multi-polarized array antenna for 5G mobile base station adopting polarization and directivity control," *IEEE Access*, vol. 6, pp. 8682–8694, 2018.
[7] W. Chen, H. Lin, H. Ding, Y. Liu, M. Chisala, Z. Shen, H. Zhibin, L. Baihui, and R. Wang, "A low profile broadband dual-polarized base station antenna using folded dipole radiation element," *IEEE Access*, vol. 7, pp. 67679–67685, 2019.
[8] B. Feng, K. L. Chung, J. Lai, and Q. Zeng, "A conformal magneto-electric dipole antenna with wide H-plane and band-notch radiation characteristics for sub-6-GHz 5G base-station," *IEEE Access*, vol. 7, pp. 17469–17479, 2019.
[9] Q. Hua, Y. Huang, C. Song, M. O. Akinsolu, B. Liu, T. Jia, Q. Xu, and A. Alieldin, "A novel compact quadruple-band indoor base station antenna for 2G/3G/4G/5G systems," *IEEE Access*, vol. 7, pp. 151350–151358, 2019.
[10] M. Li, X. Chen, A. Zhang, and A. A. Kishk, "Dual-polarized broadband base station antenna backed with dielectric cavity for 5G communications," *IEEE Antennas Wireless Propag. Lett.*, vol. 18, no. 10, pp. 2051–2055, Oct. 2019.
[11] Y. Zhu, Y. Chen, and S. Yang, "Decoupling and low-profile design of dual-band dual-polarized base station antennas using frequency-selective surface," *IEEE Trans. Antennas Propag.*, vol. 67, no. 8, pp. 5272–5281, Aug. 2019.
[12] Y. Cui, R. Li, and H. Fu, "A broadband dual-polarized planar antenna for 2G/3G/LTE base stations," *IEEE Trans. Antennas Propag.*, vol. 62, no. 9, pp. 4836–4840, Sep. 2014.
[13] Y. Gou, S. Yang, J. Li, and Z. Nie, "A compact dual-polarized printed dipole antenna with high isolation for wideband base station applications," *IEEE Trans. Antennas Propag.*, vol. 62, no. 8, pp. 4392–4395, Aug. 2014.
[14] H. Huang, Y. Liu, and S. Gong, "A dual-broadband, dual-polarized base station antenna for 2G/3G/4G applications," *IEEE Antennas Wireless Propag. Lett.*, vol. 16, pp. 1111–1114, 2017.
[15] Y. Cui, L. Wu, and R. Li, "Bandwidth enhancement of a broadband dual-polarized antenna for 2G/3G/4G and IMT base stations," *IEEE Trans. Antennas Propag.*, vol. 66, no. 12, pp. 7368–7373, Dec. 2018.
[16] Q. Zhang and Y. Gao, "A compact broadband dual-polarized antenna array for base stations," *IEEE Antennas Wireless Propag. Lett.*, vol. 17, no. 6, pp. 1073–1076, Jun. 2018.
[17] W. Shi and Q.-X. Chu, "A novel broadband low-profile base station antenna with AMC reflector," in *Proc. 6th Asia–Pacific Conf. Antennas Propag. (APCAP)*, Xi'an, China, Oct. 2017, pp. 1–3.
[18] H. Zhai, K. Zhang, S. Yang, and D. Feng, "A low-profile dual-band dual-polarized antenna with an AMC surface for WLAN applications," *IEEE Antennas Wireless Propag. Lett.*, vol. 16, pp. 2692–2695, 2017.
[19] K. Zhang, X. Zhou, Z. Wei, and H. Zhai, "A low-profile dual-band antenna loaded with the AMC surface," in *Proc. 6th Asia–Pacific Conf. Antennas Propag. (APCAP)*, Xi'an, China, Oct. 2017, pp. 1–3.
[20] X. He, B. Feng, and Q. Zeng, "A low-profile differentially feeding dual-polarized antenna using wideband AMC reflector," in *Proc. IEEE Int. Conf. Signal Process., Commun. Comput. (ICSPCC)*, Qingdao, China, Sep. 2018, pp. 1–4.
[21] M. Li, Q. L. Li, B. Wang, C. F. Zhou, and S. W. Cheung, "A low-profile dual-polarized dipole antenna using wideband AMC reflector," *IEEE Trans. Antennas Propag.*, vol. 66, no. 5, pp. 2610–2615, May 2018.
[22] H. Zhai, L. Xi, Y. Zang, and L. Li, "A low-profile dual-polarized high-isolation MIMO antenna arrays for wideband base-station applications," *IEEE Trans. Antennas Propag.*, vol. 66, no. 1, pp. 191–202, Jan. 2018.
[23] X. Zhou, J. Shi, D. Feng, and H. Zhai, "A low-profile dual-polarized mimo antenna array with high isolation," in *Proc. Int. Conf. Microw. Millim. Wave Technol. (ICMMT)*, Chengdu, China, May 2018, pp. 1–3.
[24] M. Ameen, O. Ahmad, and R. Chaudhary, "Wideband circularly-polarised high-gain diversity antenna loaded with metasurface reflector for small satellite applications," *Electron. Lett.*, vol. 55, no. 15, pp. 829–831, Jul. 2019.
[25] M. Ameen and R. Chaudhary, "Metamaterial-based wideband circularly polarised antenna with rotated V-shaped metasurface for small satellite applications," *Electron. Lett.*, vol. 55, no. 7, pp. 365–366, Apr. 2019.
[26] J. Lin, Z. Qian, W. Cao, S. Shi, Q. Wang, and W. Zhong, "A low-profile dual-band dual-mode and dual-polarized antenna based on AMC," *IEEE Antennas Wireless Propag. Lett.*, vol. 16, pp. 2473–2476, 2017.
[27] T. Yue, Z. H. Jiang, and D. H. Werner, "Compact, wideband antennas enabled by interdigitated capacitor-loaded metasurfaces," *IEEE Trans. Antennas Propag.*, vol. 64, no. 5, pp. 1595–1606, May 2016.
[28] *ANSYS HFSS: High Frequency Electromagnetic Field Simulation Software*. Accessed: Oct. 20, 2019. [Online]. Available: https://www.ansys.com/products/electronics/ansys-hfss
[29] A. Foroozesh and L. Shafai, "Investigation into the application of artificial magnetic conductors to bandwidth broadening, gain enhancement and beam shaping of low profile and conventional monopole antennas," *IEEE Trans. Antennas Propag.*, vol. 59, no. 1, pp. 4–20, Jan. 2011.
[30] *Taizhou Wangling Insulating Materials Factory-Teflon Woven Glass Fabric With Ceramic Filler Copper-Clad Laminates F4BTME-1/2*. Accessed: Oct. 20, 2019. [Online]. Available: http://www.wang-ling.com.cn/EN/products_view.asp?id=483
[31] A. Feresidis, G. Goussetis, S. Wang, and J. Vardaxoglou, "Artificial magnetic conductor surfaces and their application to low-profile high-gain planar antennas," *IEEE Trans. Antennas Propag.*, vol. 53, no. 1, pp. 209–215, Jan. 2005.

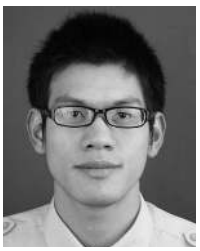

QINGCHONG LIU received the B.S. degree in physics from Nanjing Normal University, Nanjing, China, in 2012. He is currently pursuing the Ph.D. degree with the Centre for Optical and Electromagnetic Research, Zhejiang University, Hangzhou, China. His current research interests include antenna design, metamaterial, AMC, and metasurfaces.

HUI LIU (Member, IEEE) was born in Zhumadian, China. He received the M.S. degree in electromagnetic field and microwave technology from South China Normal University, China, in 2013, and the Ph.D. degree in microelectronics and solid state electronics from the Centre for Optical and Electromagnetic Research, Academy of Advanced Optoelectronics, South China Normal University, in 2018. He is currently a Postdoctoral Researcher with the Center for Optical and Electromagnetic Research, Zhejiang University. His research interests include antenna, RF circuits, and microwave components.

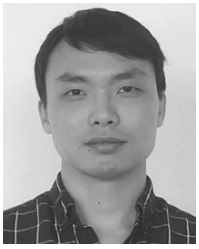

WANG HE received the B.E. degree in information engineering from Zhejiang University, Hangzhou, China, in 2015, where he is currently pursuing the Ph.D. degree with the Centre for Optical and Electromagnetic Research. His current research interests include antenna design, RFID technology, and RF EMF exposure.

SAILING HE (Fellow, IEEE) received the Licentiate and Ph.D. degrees in electromagnetic theory from the KTH Royal Institute of Technology, Stockholm, Sweden, in 1991 and 1992, respectively. He has been an Assistant Professor, an Associate Professor, and a Full Professor with the Department of Electromagnetic Engineering, KTH Royal Institute of Technology. He is also a Professor with the Centre for Optical and Electromagnetic Research, Zhejiang University, China. He has first-authored one monograph (Oxford University Press) and authored/coauthored over 600 articles in refereed international journals. He has given many invited/plenary talks in international conferences. He has served in the leadership for many international conferences. His current research interests include electromagnetic metamaterials, optoelectronics, sensing and communication.